Theoretical modelling of chromospheric emission lines through the solar activity cycles 21–23 according to the observational analysis results

Article *in* Proceedings of the Bulgarian Academy of Sciences · November 2018

DOI: 10.7546/CRABS.2018.11.10

CITATIONS
5

READS
70

1 author:

Umit Deniz Goker
The Czech Academy of Sciences
33 PUBLICATIONS **158** CITATIONS

SEE PROFILE

Доклади на Българската академия на науките
Comptes rendus de l'Académie bulgare des Sciences
Tome 71, No 11, 2018

SPACE SCIENCES
Solar physics

THEORETICAL MODELLING OF CHROMOSPHERIC EMISSION LINES THROUGH THE SOLAR ACTIVITY CYCLES 21–23 ACCORDING TO THE OBSERVATIONAL ANALYSIS RESULTS

Ümit Deniz Göker

(*Submitted by Corresponding Member P. Velinov on May 26, 2018*)

Abstract

In our previous papers, we compared the connection between the sizes of faculae and plage regions, sunspots/sunspot groups (SGs), chromospheric emission lines and solar spectral irradiance variability between the spectral ranges 121.5–300.5 nm for the period 1981–2009 and discussed the changes in the sunspot counts (SSCs) and the number of SGs relative to the variations in solar activity indices. In this work, we tried to explain the theoretical reason for these variabilities in the ultraviolet region and connected these changes to the temporal variations of solar activity indices in comparison to different type of SSCs/SGs for the first time in the literature. We found that the intensity of Fe II (298.5 nm) ion in the last solar minimum was higher than the two previous solar minima 21 and 22. So, the velocity of particles of Fe II ions increases with decreasing density of the medium and increasing plage surface. Increasing velocity causes an increase in the acceleration and intensity of particles.

Key words: Sun activity, Sun chromosphere, Sun photosphere, Sun plages

1. Introduction. Total solar irradiance (TSI) and solar spectral irradiance (SSI) are the radiative energy fluxes from the sun to the earth direction at 1 AU which are given in units of Wm^{-2} and $\mathrm{Wm}^{-2}\mathrm{nm}^{-1}$, respectively [1]. Both TSI and SSI variations will essentially be affected by the magnetic and the thermal effects (e.g. sunspots, faculae, etc.) on the solar surface [2–6]. Depending on the

DOI:10.7546/CRABS.2018.11.10

13 years length of the solar activity cycle (SAC) 23, all the physical parameters (e.g. magnetic flux, sunspot number, facular activity, Mg II index and 10.7 cm solar radio flux) were lower than the two previous cycles 21 and 22. The most distinctive decreases were seen in the area of bright faculae and chromospheric plages for the SAC 23 [7] and it caused the decrease of the ratio between facula and plage, and the magnetic field intensity became smaller. However, the area covered by facular areas (FAs) on the solar surface was the largest in 1990 in SAC 22, while it was the lowest in 2001 in SAC 23. The total (and the average) areas of plages decreased in both the decreasing and the increasing phases of SAC 23 [8].

The particle velocities measured in plages and FAs are mainly due to the magnetic field intensity and the temperature [8,9]. If the number of plage regions on the solar surface is low and the areas covered by plages are large, this would indicate the presence of much lower magnetic field, as seen in SAC 23. By the end of 2008, sunspots and solar irradiance had reached their lowest levels for the minimum phase of SAC 23 [10], but this decreasing did not stop the increase of the SSI intensity from 289.5 nm to 300.5 nm in the ultraviolet (UV) region [9]. We found from our data analysis results that there is a negative correlation between the intensity of UV spectral line corresponding to the 298.5 nm wavelength of Fe II ion originating from the solar chromosphere and the international sunspot number (ISSN) index corresponding to the minimum phase between the SACs 22 and 23 [8,9]. In addition, a similar abnormal increasing has also been found with the studies of helioseismology [11], which has led us to the conclusion that the main increase is caused by a chemical change in the interior of the sun.

As a result of these studies, we *only* found Fe II (298.5 nm emission line) ion with very high ionization level because of the association of the ionization phase with the velocity of particles, and the decrease in the intensity due to the increase of the ionization phase with increasing velocity [12]. In our previous paper, we searched which solar activity indices show the most probable changes by comparing the observational data that shows the changes in sunspots/sunspot groups (SGs), Ca II K-flux, facula and plage regions with the standardized time series analyzes of SSI and ISSN data, and we found that the distinct change originated from the plage regions [9].

In this work, considering that one of these certain areas corresponds to a single and special plage region in the solar chromosphere, we created a general intensity equation by taking reference of the acceleration of charged particles in a single plage region and the total particle acceleration of all other plage regions on the solar surface.

2. Basic equations and theoretical method. The total amount of radiation is given by the product of the average disk intensity with the total area of the solar disk [13]. The radiation intensity is given by

$$I = \langle \mathbf{S} \rangle = \frac{P_{\text{net}}}{A} = \frac{P_e - P_a}{A} = \varepsilon\sigma \left[T_e^4 - T_a^4\right] = \varepsilon\sigma T_{\text{net}}^4, \tag{1}$$

where I indicates the average disc intensity and equals the time average of the Poynting vector $\mathbf{S}$, P_{net}, A and T_{net} indicate the net power radiated, total area of the solar disk and radiation temperature, respectively. The subscripts e and a correspond to the emitted and absorbed radiation, respectively. In Eq. (1), ε indicates the emissivity parameter while σ is the Stefan's constant and equals 5.669×10^{-8} $\text{Wm}^{-2\circ}\text{K}^{-4}s^{-1}$. When the stretch of the solar cycle gets longer (e.g. SAC 23), the average temperature and the magnetic field intensity decrease. Decreasing temperature will cause the decrease of the radiation and the intensity with the increasing emissivity. Nevertheless, the intensity was not among the lower values for the last solar cycle minima in spite of the decreasing temperature. Therefore, we can mention that the increase of intensity was not affected directly by the temperature.

Having considered that one of these special structures corresponds to a single and special plage area in the solar chromosphere, we created a general intensity equation with reference to an acceleration of the charged particles in a single plage region and the total particle acceleration of all other plage regions on the solar surface. All electric field lines radiate away from the origin in all directions (Fig. 1a) while outside of a sphere of radius $r \sim ct$ (in our work, this radius corresponds to equally divided patterns on the solar disc and it is shown in Fig. 2) the field lines still indicate the position of the charge with respect to the origin while the field lines point the new location of the charge after the acceleration inside this sphere. In this figure, the X-direction denotes the direction of the moving charge perpendicular to the electric field while the Y-direction denotes the direction of the acceleration vector with respect to the line of sight.

$$E_\theta = \Delta V t \sin\theta, \tag{2}$$

where θ is the angle between the acceleration vector and the line from the charge to the observer, and E_θ indicates the tangential component of the electric field. From the dipolar form of the energy loss (Fig. 1b), E_r is the radial component of the electric field.

$$E_r = c\Delta t = \frac{q}{r^2}. \tag{3}$$

The ratio of electric fields gives

$$E_\theta = \frac{q}{r^2}\left(\frac{dV}{dt}\right)\frac{r\sin\theta}{c^2} = \frac{q\dot{V}}{rc^2}\sin\theta. \tag{4}$$

The Poynting vector of the electromagnetic wave is given by [14]

$$|\mathbf{S}| = \frac{c}{\mu_0}|\mathbf{E}\times\mathbf{B}| = \frac{c}{4\pi}|\mathbf{E}\times\mathbf{B}|, \tag{5}$$

where c is the speed of light, μ_0 is the vacuum permeability, $\mathbf{E}$ is the electric field and $\mathbf{B}$ is the magnetic field. For our plane transverse electromagnetic waves, the fields $\mathbf{E}$ and $\mathbf{B}$ are perpendicular to the direction of $\mathbf{S}$.

$$|\mathbf{S}| \equiv \frac{dW}{dtdA} = \frac{c(EB)}{4\pi} = \frac{c}{4\pi}E_\theta^2 = S, \tag{6}$$

where W is the radiated energy and A is the total area of the solar disk. This equation gives the rate of energy flow per unit area in a given direction measured in $\mathrm{Wm^{-2}s^{-1}}$. The charge radiates with a dipolar ($\sin\theta$) power pattern whose axis is parallel to $\dot{V}$ [14] as shown in Fig. 1b. Integrating the power over the whole area ($dA = r^2 d\Omega$) on the surface of the sphere, we get the total power radiated. Here, $d\Omega = \sin\theta d\theta d\varphi$ is the surface element of a sphere. The angles θ and ϕ are the spherical coordinates in the surface element of the sphere which is shown in Fig. 2. The total power radiated can be written by using the Poynting flux in the sphere by integrating Eq. (7) over all directions

$$P \equiv \frac{dW}{dt} = \int_{\mathrm{sphere}} |\mathbf{S}|\, dA. \tag{7}$$

So, Eqs (4)–(8) represent Eq. (9), where q is the charge and equals eZ, where e and Z indicate the electron charge and the atomic number of the nucleus, respectively.

$$P = \int_{\mathrm{sphere}} \frac{c|\mathbf{E}\times\mathbf{B}|}{4\pi}\, dA = \frac{c}{4\pi}\int_{\mathrm{sphere}} E_\theta^2\, dA = \frac{c}{4\pi}\int_{\mathrm{sphere}} \left(\frac{q\dot{V}}{rc^2}\sin\theta\right)^2 dA, \tag{8}$$

$$P = \int_{\varphi=0}^{2\pi}\int_{\theta=0}^{\pi} \frac{q^2\dot{V}}{4\pi c^3}\left(\frac{\sin^2\theta}{r^2}\right) r^2\sin\theta\, d\theta\, d\phi = \frac{q^2\dot{V}^2}{4\pi c^3}\int_{\theta=0}^{\pi}\sin^3\theta\, d\theta. \tag{9}$$

For $dV/dt = a$ (acceleration), Eq. (9) equals

$$P = \frac{2}{3}\frac{q^2a^2}{c^3}. \tag{10}$$

This equation describes the total power radiated from electric dipole radiation by a non-relativistic particle. Since the particle has an angular velocity originating from the kinetic energy due to its acceleration, we need to add the angular velocity value that we find out from the equation of motion

$$\omega_B = \frac{qB}{m_i c} = \frac{ZeB}{m_i c}. \tag{11}$$

Here, the particle charge equals $e = 4.803\times10^{-10}$ esu, and m_i is the mass of Fe II ions. As a result, the total amount of power generated by combining Eqs (1), (10) and (11) into a single plage region is calculated from the *Larmor* formula

$$P_p = \frac{2q^2}{3c^3}|\mathbf{a}_p|^2 = \frac{2q^2}{3c^3}\times\left(\frac{qV_{\perp p}B_p}{m_{ip}c}\right)^2 = \frac{2(Ze)^4}{3c^5}\left(\frac{(V_{\perp p})^2B_p^2}{(m_{ip})^2}\right), \tag{12}$$

where P_p indicates a single plage region.

If we want to calculate the total plage areas on the solar surface and the total amount of power radiated from these areas, we write

$$I_{\text{Top}} = \sum \frac{P_{\text{Top}}}{A_{\text{Top}}} = \sum \frac{P_{p1}}{A_{p1}} + \frac{P_{p2}}{A_{p2}} + \frac{P_{p3}}{A_{p3}} + \cdots + \frac{P_{pn}}{A_{pn}}, \tag{13}$$

$$I_{\text{Top}} = \frac{2(Ze)^4}{3c^5} \sum_{i=1}^{n} \left[\left(\frac{(V_{\perp p})_1^2 B_{p1}^2}{(m_{ip})_1^2 A_{p1}^2} \right) + \left(\frac{(V_{\perp p})_2^2 B_{p2}^2}{(m_{ip})_2^2 A_{p2}^2} \right) + \left(\frac{(V_{\perp p})_3^2 B_{p3}^2}{(m_{ip})_3^2 A_{p3}^2} \right) + \cdots + \left(\frac{(V_{\perp p})_n^2 B_{pn}^2}{(m_{ip})_n^2 A_{pn}^2} \right) \right]. \tag{14}$$

The unknown parameters in Eq. (14) are $(m_{ip})_1^2 \to (m_{ip})_n^2$, $B_{p1}^2 \to B_{pn}^2$, $A_{p1}^2 \to A_{pn}^2$ and $(V_{\perp p})_1^2 \to (V_{\perp p})_n^2$, and these values are the parameters that will change for each observation time in each solar cycle, in each plage region. Here, $(m_{ip})_1$, B_{p1}, A_{p1} and $(V_{\perp p})_1$ show the ion mass, magnetic field intensity, area of pattern and perpendicular velocity for Fe II ion in one square-like area while $(m_{ip})_n$, B_{pn}, A_{pn} and $(V_{\perp p})_n$ show the ion mass, magnetic field intensity, area of pattern and perpendicular velocity for Fe II ion in total square-like areas which corresponds to the total area of plage region, respectively. We will use expansion in a series to solve Eq. (14) depending on the number of square-like areas. From this calculation, we will find the total intensity coming from the totality of square-like areas. We used the cartesian coordinate system corresponding to the geometry of the total power emitted by an accelerated charged particle to solve Eq. (14) depending on the number of square-like areas. The power received in equally divided patterns (square-like areas) in any direction is proportional to the component of $\dot{V}$ perpendicular to the line-of-sight, so the perpendicular velocity, $V_{\perp p}$, is used in our general equation. From the Larmor formula, a charged particle having a velocity vector that has a component parallel to a uniform magnetic field moves in a helical path and the plane is perpendicular to the magnetic field in Fig. 1 and 2, and Eq. (14).

3. Results and discussions. In our previous papers, we investigated the SSI intensities in the range 121.5–300.5 nm for SACs 21, 22 and 23 obtained by Solar Mesosphere Explorer (SME), Upper Atmosphere Research Satellite (UARS) and The Solar Radiation and Climate Experiment (SORCE) experiments. Time series of SSI have been extracted from data centers of National Space Science Data Center (NSSDC), Goddard Distributed Active Archive Center (GDAAC) and LASP Interactive Solar Irradiance Data Center (LISIRD) that served the archives of NASA space mission data. These different interactive data centers have taken the observational data for each 0.5 nm in the UV spectral range, so we made our analysis for each 0.5 nm wavelength interval. The ISSN data were obtained from the Solar Influences Data Analysis Center (SIDC) and World

Data Center for the Sunspot Index, at the Royal Observatory of Belgium. All the spectral lines between the ranges 121.5–300.5 nm and 200.5–300.5 nm were taken from the Harrison atlas and the work [15], respectively. In this respect, we revealed negative correlations of intensities of UV (289.5–300.5 nm) spectral lines originating in the solar chromosphere with the ISSN index during the unusually prolonged minimum between the SACs 23 and 24. We compared our results with the variations of solar activity indices (e.g. TSI, magnetic activity, Ca II K-flux, faculae and plage areas) obtained by the ground-based telescopes and a time series method was done to explain the unexpected variation in solar activity indices in the last solar activity cycle (SAC 23) [8,9].

All SG classification data were taken from the National Geographical Data Center and they include various observational parameters of SGs and SSCs for each group recorded during the observed day. The data were collected by the United States Air Force/Mount Wilson Observatory (USAF/MWL). We used the Rome Astronomical Observatory (ROME) and the Learmonth Solar Observatory (LEAR) data as the principal data source for SAC 21, SACs 22 and 23, respectively. Zurich classification for cycle 21 and the modified Zurich (McIntosh) classification data for cycles 22–23 and the first half of cycle 24 were used. The data for TSI and full disk magnetic activity of the Sun were taken from SOLAR 2000 data and Wilcox Solar Observatory, respectively. The data for faculae and Ca II K-line were based on daily synoptic full-disk images obtained by photoelectric photometry of sunspots at the San Fernando Observatory (SFO). The plage and Ca II K-flux observations were taken from the Kodaikonal Data (KKL). Detailed analysing techniques can be found in [8,9].

Although all the properties of the SAC 23 conform to the structure of solar activity, an increase was observed in the intensity of UV region for certain wavelengths. This indicates that the increase of intensity is a direct change in the inner structure of the sun rather than being affected by temperature or surface parameters. Helio-seismic data have also shown a surprising anti-correlation between frequencies and activity proxies during the minimum between SACs 23 and 24. The heavy element abundances affect the helio-seismology by causing changes in the convection zone-structure, and changes in the convection zone will affect the radiative opacities, the boundary between the radiative and convection zones and the equation of state [8]. Normally, the helio-seismic oscillations are associated with the inner part of the Sun while we are working on the upper photopshere and chromosphere of the Sun. However, our suggested theory is also proved by the discrepancy of SAC 23 with helioseismological study [11] and they found similar abnormal increases in their analysis. We thought that if something exists inside the Sun, it can easily affect the atmospheric layers. In particular, the possible changes in plages, as well as the chemical effects of internal structure that cause these regions to change, will also affect the chromospheric radiation. These effects will be even more important for wavelengths below 400 nm since

the bound-bound absorption of metallic lines below 400 nm has a very important effect on the optical thickness, and rapid changes in the UV spectral region firstly affect the heavy element ions.

From our data analysis results, we found a negative correlation of intensity of the UV (from 289.5 nm to 300.5 nm) spectral line (corresponding to the Fe II chemical element ion in 298.5 nm) originating in the solar chromosphere with the ISSN index during the minimum between SACs 23 and 24. Similar results for UV spectral lines have been obtained by [11] using five years of daily EUV spectral data recorded by the TIMED/SEE (NASA Thermosphere Ionosphere Mesosphere Energetics and Dynamics/Solar EUV Experiment) satellite. In the UV ranges of the spectrum, chromospheric metal ions are especially increased and this increase is more powerful for the metal iron for the decreasing phases of SACs 22 and 23 (298.5 nm). So, any physical changes (e.g. the velocity, acceleration, the density, and the radius of the medium) that will occur in the UV region substantially affect the heavy element ions [8].

In order to prove our theoretical model, the best is to perform the spectral analysis corresponding to the wavelength of 298.5 nm. We need analytical solutions of spectral data exchange for iron and iron group elements in the solar composition; in our future work we will prove the theory that we have proposed in Eq. (14) by looking at whether the other spectral data observations match our spectral data or not for SACs 21–23.

4. Conclusions. The goal of our study is to investigate the anomalous activity from the beginning of SAC 23 which can play a significant role in the further development of SAC 24 and in the forecasting of activity parameters for the future cycles. In SAC 23, the surfaces covered by plages on the Sun were smaller and this might have caused the increase of the ratio between facula and plage, and the magnetic field flux from the Sun was lower. The most important decrease for the total and average area of plages was seen in the decreasing phase of SAC 23, but in spite of this Fe II (298.5 nm) chromospheric ion in the UV region showed a distinctive increase. From these results, we can say that plage regions and the emergence of the magnetic flux from the Sun have shown the most distinctive variations between SACs 21–23 than the other solar activity indices. The other chromospheric ions such as C II, Co II, Cr II, Mg II, Mn II, Ni II and Ti II in other wavelengths also affect the intensity but not so much as the Fe II ion because the highest ionization level only occurs for the metal iron [8]. Ionization level is related with the velocity: it becomes higher as the velocity increases and the density decreases. Increasing velocity also causes the increase of the acceleration and intensity.

Therefore, this increasing caused us to investigate different phenomena from the previous studies, and we tried to connect this increase of the SSI intensity with the classes and the numbers of sunspots/ sunspot groups, faculae and plage regions, and Ca II K-index and thereby investigate the possible elements corre-

sponding to these wavelength ranges and examine whether these elements affect the increase or not.

Most systems found in nature are not in thermodynamic equilibrium because they are changing or can be triggered to change over time, and are continuously and discontinuously subject to fluxes of matter and energy to and from other systems. The thermodynamic study of non-equilibrium systems requires more general concepts than are dealt with by equilibrium thermodynamics. This is why photospheric and faculaer physical models have been derived by calculations in non-local theromodynamic equilibrium (non-LTE or NLTE) [16].

Our general equation (14) indicates the total intensity coming from the plage region on the Sun. In the UV region and at the temperatures lower than 2×10^4 K which the chromospheric emission lines formed, there is no local thermodynamic equilibrium and the source function can no longer be considered to be a Planck function as mentioned by [16–18]. Therefore, we can combine Eq. (14) with equations ([16], (3)), ([17], (1)), ([18], (1)), respectively. In these equations the total source function $S_j(\Delta\lambda)$ equals the sum of the depth variation of the line source function (S_l) and continuum source function (S_c), and $S_j(\Delta\lambda)$ is obtained by simultaneously solving the equation of radiative transfer and the equation of statistical equilibrium. The new equation generated by the addition of the equations given in [16–18] to our general Eq. (14) will be formed in our next paper and analytical solutions will be done as well.

Acknowledgements. The authors would like to thank Prof. Dr. G. B. Rybicki and Prof. Dr. A. P. Lightman from the Harvard-Smithsonian Center for Astrophysics and Massachusetts Institute of Technology. The authors also would like to thank the anonymous referee(s) for valuable comments and guidance.

REFERENCES

[1] Parker D. G. (2010) PhD Thesis, University of California.
[2] Foukal P. (1992) Solar luminosity variation, The solar cycle. In: Proc. Nat. Solar Observatory/Sacramento Peak 12th Summer Workshop, ASP Conf. Ser. (ASP: San Francisco), **27**, 439.
[3] Chapman G. A., A. M. Cookson, J. J. Dobias (1996) Variations in total solar irradiance during solar cycle 22, J. Geophys. Res., **101**, 13541–13548.
[4] Fligge M., S. K. Solanki, Y. C. Unruh, C. Fröhlich, Ch. Wehrly (1998) A model of solar total and spectral irradiance variations, Astronomy & Astrophysics, **335**, 709–718.
[5] Fligge M., S. K. Solanki, Y. C. Unruh (2000) Modelling irradiance variations from the surface distribution of the solar magnetic field, Astronomy & Astrophysics, **353**, 380–388.
[6] Krivova N. A., S. K. Solanki, M. Fligge, Y. C. Unruh (2003) Reconstruction of solar irradiance variations in cycle 23: Is solar surface magnetism the cause?, Astronomy & Astrophysics, **399**, L1–L4.

[7] de Toma G., O. R. White, G. A. Chapman, S. R. Walton, D. G. Preminger et al. (2004) Solar cycle 23: An anomalous cycle, Astrophys. J., **609**, 1140–1152.
[8] Göker Ü. D., M. Sh. Gigolashvili, N. Kapanadze (2017) Solar spectral irradiance variability of some chromospheric emission lines through the solar activity cycles 21–23, Serbian Astronom. J., **194**, 71–86.
[9] Göker Ü. D., J. Singh, F. Nutku, M. Priyal (2017) Temporal variations of different solar activity indices through the solar cycles 21–23, Serbian Astronom. J., **195**, 59–70.
[10] Gibson S. E., G. de Toma, B. Emery, P. Riley, L. Zhao et al. (2011) The whole heliosphere interval in the context of a long and structured solar minimum: an overview from sun to earth, Solar Physics, **274**, 5–27.
[11] Amblard P.-O., S. Moussaoui, T. Dudok de Wit, J. Aboudarham, M. Kretzschmar et al. (2008) The EUV sun as the superposition of elementary suns, Astronomy & Astrophysics, **487**, L13–L16.
[12] Liu W., D. J. Jeffery, D. R. Schultz (1998) Ionization of Type Ia supernovae: Electron impact, photon impact, or charge transfer?, Astrophys. J., **494**, 812–815.
[13] Fontenla J., O. R. White, P. A. Fox, E. H. Avrett, R. L. Kurucz (1999) Calculation of solar irradiances. I. Synthesis of the solar spectrum, Astrophys. J., **518**, 480–499.
[14] Rybicki G. B., A. P. Lightman (2004) Radiative Processes in Astrophysics, Harvard Smithsonian Center for Astrophysics, Wiley-VCH Verlag GmbH & Co. KGaA, 1–312.
[15] Doschek G. A., U. Feldman, L. Cohen (1977) Chromospheric limb spectra from *SKYLAB*: 2000 to 3200 Å, Astrophys. J. Suppl. Ser., **33**, 101–111.
[16] Semeida M., B. Marzouk, P. Stoeva, A. Stoev (2016) Physical models for Ca II IR triplet lines in solar photosphere and faculae in non-local thermodynamic equilibrium, C. R. Acad. Bulg. Sci., **69**(8), 1047–1056.
[17] Semeida M., B. Marzouk, P. Stoeva, A. Stoev (2015) Empirical investigation of solar photosphere and faculae in Ca II IR triplet lines using non-local thermodynamic equilibrium model, C. R. Acad. Bulg. Sci., **68**(10), 1287–1294.
[18] Abseim A., M. Semeida, M. Saleh, S. Youssef, P. Stoeva et al. (2017) Modified cloud method validation by determination of physical parameters of the solar flare on June 26, 1999, C. R. Acad. Bulg. Sci., **70**(6), 839–848.

Department of Aviation Management
Faculty of Economics, Administrative
and Social Sciences
Istanbul Gelişim University
Avcılar, 34315 Istanbul, Turkey
e-mail: udgoker@gelisim.edu.tr

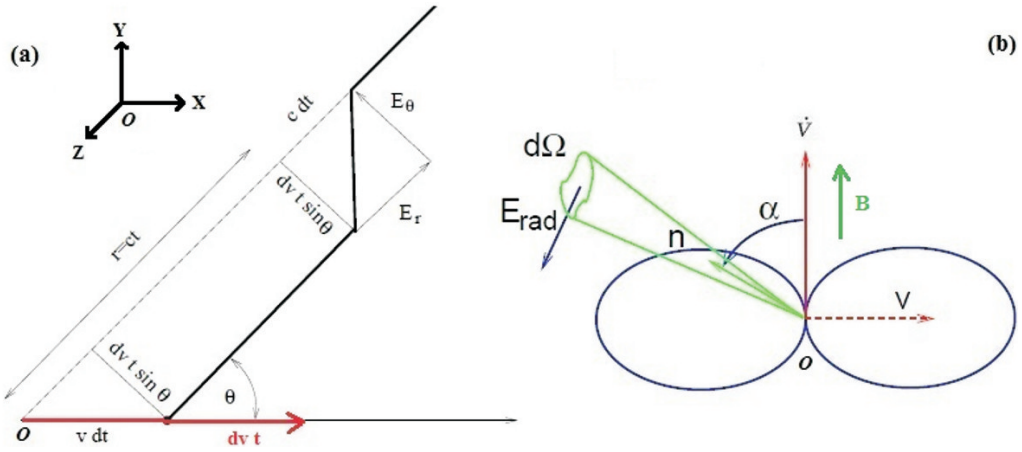

Fig. 1. (a) The geometry of the electric fields. Here the X-direction denotes the direction of the moving charge perpendicular to the electric field and the Y-direction denotes the direction of the acceleration vector with respect to the line of sight. (b) Dipolar form of the energy loss. Here α is the pitch angle of $\mathbf{V}$ with respect to the magnetic field $\mathbf{B}$. For circular motion, the velocity perpendicular to the magnetic field equals $V_{\perp} = V \sin\alpha$. For pure circular motion $V_{//} = 0$ and the pitch angle equals $\alpha = \pi/2$ (courtesy of [14])

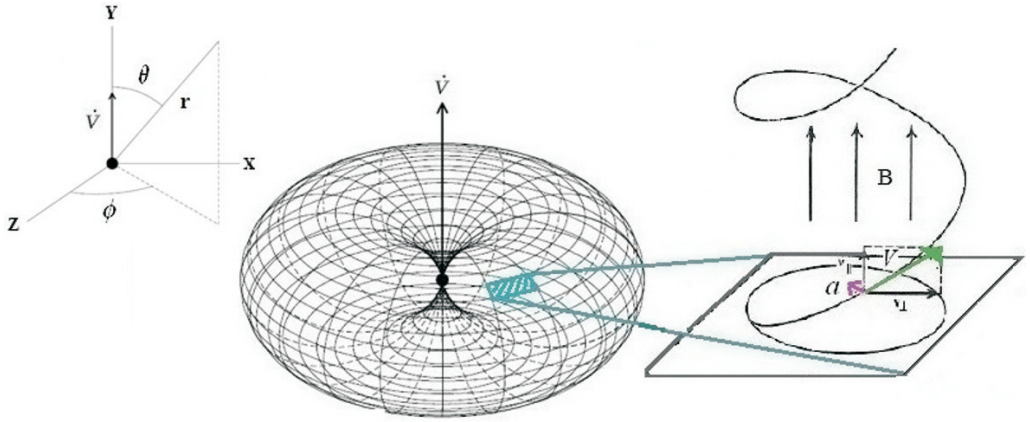

Fig. 2. The cartesian coordinate system corresponds to the geometry of the total power emitted by an accelerated charged particle. The power received in equally divided patterns in any direction is proportional to the component of $\dot{V}$ perpendicular to the line-of-sight. The TSI variations are determined by the sum of the power received from all these patterns separately. We assume that one of these patterns corresponds to a particular area of one plage region on the solar chromosphere. A charged particle having a velocity vector that has a component parallel to a uniform magnetic field moves in a helical path and the plane is perpendicular to the magnetic field (courtesy of [14])